

RESEARCH ARTICLE

Engineering of core/shell nanoparticles surface plasmon for increasing of light penetration depth in tissue (modeling and analysis)

Sona Faalnouri¹; Ahmad SalmanOgli^{2*}

¹Biochromatography and Biodiagnostics Research Laboratory, Chemical Department, Hacettepe University, Ankara, Turkey

²Photonics and Nanocrystal Research Laboratory, Electrical Engineering Department, University of Tabriz, Tabriz, Iran

ARTICLE INFO

Article History:

Received 01 August 2017

Accepted 20 September 2017

Published 10 October 2017

Keywords:

Plasmonic

Core/shell nanoparticles

Light penetration

Monte Carlo

ABSTRACT

Objective(s): In this article, a new procedure for increasing the light penetration depth in a tissue is studied and simulated. It has been reported that the most important problem in biomedical optical imaging relates to the light penetration depth, and so this makes a dramatic restriction on its applications. In the optical imaging method, the detection of the backscattered photons from a deep tumor is rarely done or is done with a low efficiency; it is because of the high absorption and scattering losses.

Methods: Unlike the common methods (using a high energy laser for deep penetration) by engineering the nanoparticles' optical properties such as their anisotropy, absorption, and scattering efficiency, which are distributed into a tissue, the detected photons amplitude can be manipulated. In other words, by engineering the nanoparticle plasmon properties and their effect on the dye molecules' quantum yield, fluorescence emission and more importantly influence on the scattering direction, the light penetration depth is dramatically increased.

Results: The modeling results (Monte-Carlo statistical method) illustrate that the detected photons dramatically increased which is on order of 4 mm. So, this method can fix the light penetration problems in the optical imaging system.

Conclusions: Finally, the original idea of this study attributes to the indirect and transient manipulation of the optical properties of the tissue through the nanoparticles plasmon properties engineering. Moreover, by engineering plasmonic nanoparticles, maybe, the penetration depth can be enhanced which means that we can easily send light into a soft tissue and get its back scattering.

How to cite this article:

Faalnouri S, SalmanOgli A, Engineering of core/shell nanoparticles surface plasmon for increasing of light penetration depth in tissue (modeling and analysis). *Nanomed Res J*, 2017; 2(3):189-198. DOI: 10.22034/nmrj.2017.03.007

INTRODUCTION

In recent years, there have been several different imaging methods for diagnosis and detection of cancer, which have been used in biomedical applications such as magnetic resonance imaging (MRI), positron emission tomography (PET), computed tomography (CT) and optical imaging (OI). Each of these methods has some advantages and disadvantages based on their applications. For instance, the MRI does not have any drawbacks

in the case of tissue depth, but it has a limited sensitivity in the case of small object detection. So, detection of smaller tumors with a radius smaller than 1 mm could not be distinctly recognized by MRI [1-7]. The OI method is another attractive method because of its high sensitivity to detect small tumors. However, this method is severely limited due to the fact that light cannot easily penetrate into tissue due to the scattering and

* Corresponding Author Email: tirdad.zey@gmail.com



This work is licensed under the Creative Commons Attribution 4.0 International License.

To view a copy of this license, visit <http://creativecommons.org/licenses/by/4.0/>.

absorption introduced by Hemoglobin and fatty and so on. To improve the OI methods' features, one can use the nanoparticle (NPs) or dye molecules as fluorophores [8-10] to enhance the incidence photons. It is notable that the deep tumor tissue detecting is very hard although we established the improved version of OI method. It is undeniable that early detection of malignant tumors is necessary, due to an increase of survival and better manipulation outcomes. It has been reported that in the initial stage of tumors or neocapillaries formation, their hypoxic and acidic condition is poor; and maybe with detection and treatment of it in the embryonic state, the invasive tumors can be controlled [4, 5, 11-18]. According to reports based on small tumor imaging and treatments, we have found that the increasing the light penetration into the tissue is an indispensable task. It is because by an improved OI method one can easily detect the small tumors. Our study proposes a unique idea in which the light propagation depth is dramatically increased in the real tissue. In fact, the original aim is the indirect and transient manipulation of the optical properties of the tissues including scattering coefficients (μ_a), absorption coefficients (μ_s), and the cosine of scattering angle (g). For this, we need to transiently change the optical tissue properties, and so the effective medium theory [19] concepts can be used. By inserting NPs into tissue, the optical parameters of the modified tissue (tissue plus NPs) are altered, which is modeled by the Monte Carlo (MC) weight constant (f_{NPs}) and NPs' optical properties such as scattering coefficients (μ_{aNPs}), absorption coefficients (μ_{sNPs}), and the cosine of scattering angle (g_{NPs}). It should be noted that f_{NPs} indicates the selection of the tissue's ingredient type and is not a fraction of inserting NPs into tissue. For instance, we used $\sim 10^9$ particles/mL in the maximum state of $f_{NPs} = 0.98$. So, for controlling the optical properties of the modified tissue, it is enough to manage the optical properties of NPs. In this research, two types of core/shell NPs (NPs_E and NPs_F) are used; one of them is used to enhance the absorption of the excitation wavelength around ~ 530 nm and another is applied to intensify the fluorescence emission at wavelength ~ 630 nm. It is obvious that in the excitation wavelength, the penetration of light in a real tissue is very limited and is smaller than 1mm. Notably, in this study, the surface plasmon resonance (SPR) hybridization

is used as an important key. The first category of NPs (Au/SiO₂/Ag-dye) is considered for some special aims: first, to increase the absorption rate of excitation photons due to the enlargement of the plasmon coupling to the tissue, and enhancing the dye molecules' quantum yield (maximum overlap with dye molecules' absorption spectra); and second, engineering of scattering events in the forward direction by changing of the medium anisotropy in which the light penetration depth is dramatically magnified. However, the second category of NPs (SiO₂/Au-dye) is designed to have several unique properties: the forward scattering direction (g_{NPs} approaching 1); enhancing the dye molecules' fluorescence (maximum overlap with dye molecules' fluorescence); and low scattering and absorption coefficients due to the decreasing loss in the propagation route. Indeed, by inserting NPs-dye in the medium, the rate of converting photons to the fluorescence state is increased and so because of introducing some specific conditions for NPs, such as the forward scattering direction, most of the dye's fluorescence photons will be registered by the detector. For simulation of the optical properties of NPs and their features, and propagation of light in the tissue, the MIE theory [20-23] and the iterative indirect methods [22-24] are used, respectively. Some suppositions of our study are: the considered NPs are non-toxic and transiently inserted into tissue; the number of episode photons per MC runs is 15,000; tissue depth and width are 2 mm for the normal condition and will be increased to 5 mm in our study.

THEORETICAL AND BACKGROUNDS

In this section, a short review of theoretical and background subsection of our study is presented. At first, optical properties of the biological tissue (a typical case for this study) is reported. In the following, for simulation and modeling of the light propagation into tissue, the MC method is introduced and finally the calculation of the cosine of the scattering angle for NPs via using the MIE theory is reported.

Optical properties of Biological tissue

We initially study the propagation of light into tissue, it is because of its critical role in different biological applications such as imaging, sensing, and targeting. Numerous methods, including

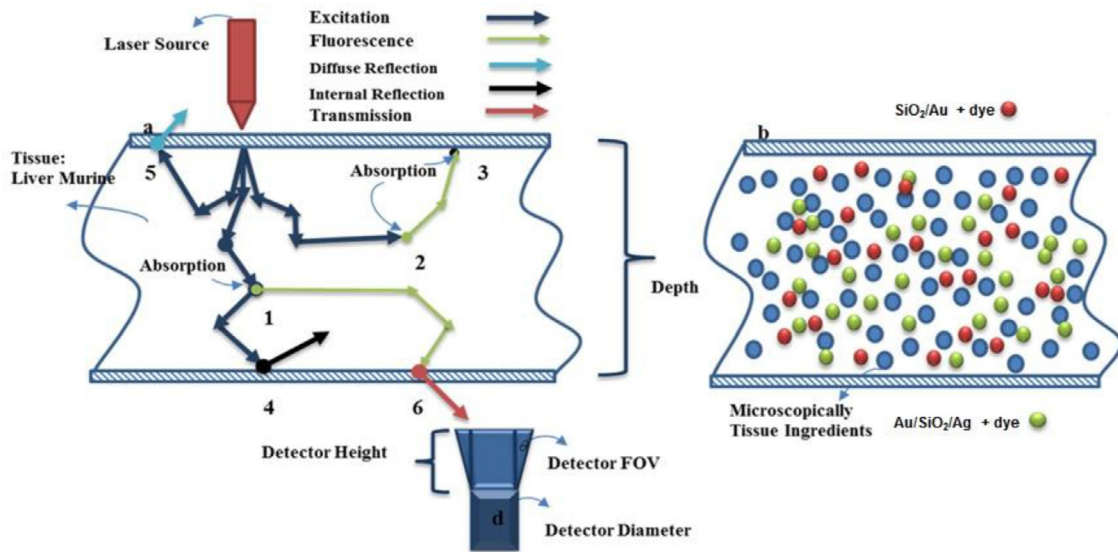


Fig. 1. (a) Schematic of the interaction of light with tissue (Absorption, scattering, diffuse reflection, Internal reflection, and transmission) and (b) microscopic view of the tissue's ingredients and randomly diffusion of NPs into tissue.

analytical, numerical and statistical have been expanded for prediction of light propagation in tissue. Optical properties are obtained by using the measured parameters: reflection, transmission, and absorption and converting into parameters which characterize the light propagation in tissue. It has been studied that describing the laser transfer into tissue is supported by the transport theory [25, 26]. Transport coefficients can be derived from the interaction of a plane wave with a particle, so a percent of waves are absorbed some are scattered and some of them are unperturbed and transmitted. It seems that the transport equation is one of the complete procedures for the definition of the tissue optical parameters and propagation of light in tissue. In the following, the measurements of the optical properties of tissue by different methods are investigated and eventually, the MC method as a candidate is considered and studied in details. Recently, several methods have been considered for measuring the optical properties of tissues. These can be categorized into two sections: direct and indirect. The direct method is the simple one and uses only nothing more complicated than the Beer's law. However, a theoretical model of the light scattering is used in the indirect method. This method can be divided into two categories such as iterative and non-iterative methods. Such methods e.g. Kubellka-Munk equations require simple expressions relating the optical properties

to measure transmission and reflection. With solving the Kubellka-Munk equations the related coefficients are given by:

$$\mu_a = \eta A_{km}, \quad \mu_s = \chi S_{km}, \quad \mu_s \cdot (1-g) = \chi' S_{km} \quad (1)$$

The optical properties (absorption, scattering, and anisotropy factor) can be concluded from Eq. 1 and moreover, by use of the provided expression for η and χ in [25] the transport coefficients can be handled. Other non-iterative methods have been used similarly. Unlike non-iterative techniques, iterative one uses complicated solutions. In this section, MC method as an iterative method which uses a statistical approach to calculate the optical properties of tissue or light propagation in the tissue is presented. In our study, optical properties of the factual tissue are used from the *in vitro* and *in vivo* results [25] and just the propagation of light in tissue is investigated and considered.

Monte Carlo method

MC refers to a technique which simulates physical processes using a stochastic model. In a radiative transport problem, the MC method consists of recording photon histories as they are scattered and absorbed. This method discussed the reflection of a photon from boundaries, and showed how the phase function maybe used to generate new scattering angle and so on. The MC method is attractive because it is easily

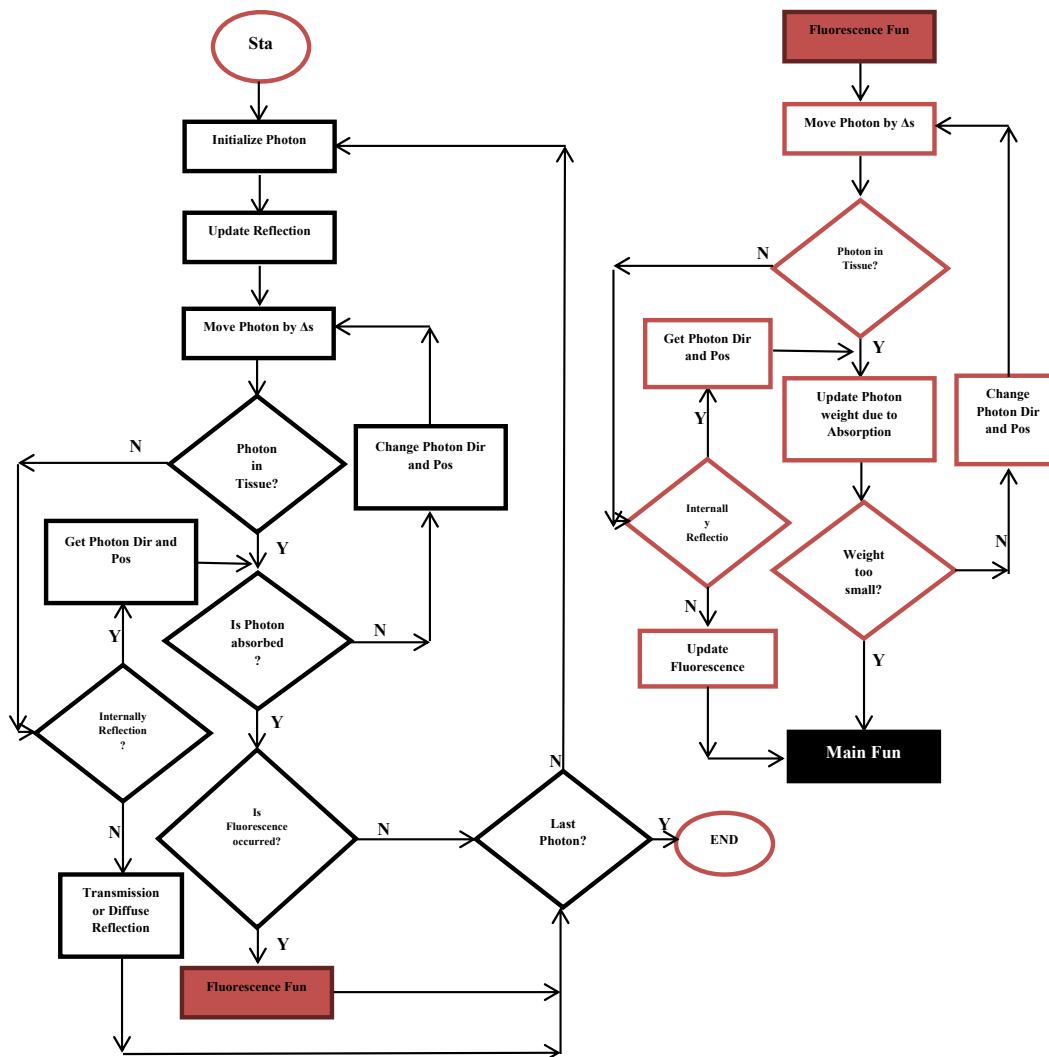


Fig. 2. MC Method Algorithm Flow Chart; Dir: direction, Pos: position; “N” and “Y” stand for No and Yes respectively.

implemented and sufficiently flexible by which the complex tissues may be modeled. It is notable that the accuracy of this method is proportional to $1/(N)^{0.5}$ where N is the number of the propagated photons. In this work, MC accuracy is considered about of 0.008. Moreover, the variable step size for each propagation step is used. MC approach begins by launching a photon downwards into the tissue at the origin. If a collimated beam is normally incident on a slab, the photon is initially directed downward into the tissue. If the incident light is diffuse, then the photon direction is chosen randomly from all possible directions in the downward hemisphere. Once launched, the photon has moved a distance

Δs where it may be scattered, absorbed, propagated undisturbed, internally reflected, or transmitted out of the tissue (Fig. 1a). The photon is repeatedly moved until it either escapes from or is absorbed by the tissue. If the photon escapes from the tissue, the reflection or transmission of the photon is recorded or if the photon is absorbed the position of absorption is recorded, and fluorescence emission is launched with latter absorbed positions. This process is repeated until the desired number of photons has been propagated (one can observe MC method algorithm flow chart illustrated in fig. 2). In this algorithm, the distance (Δs) is chosen in such a way that it is the distance at which the

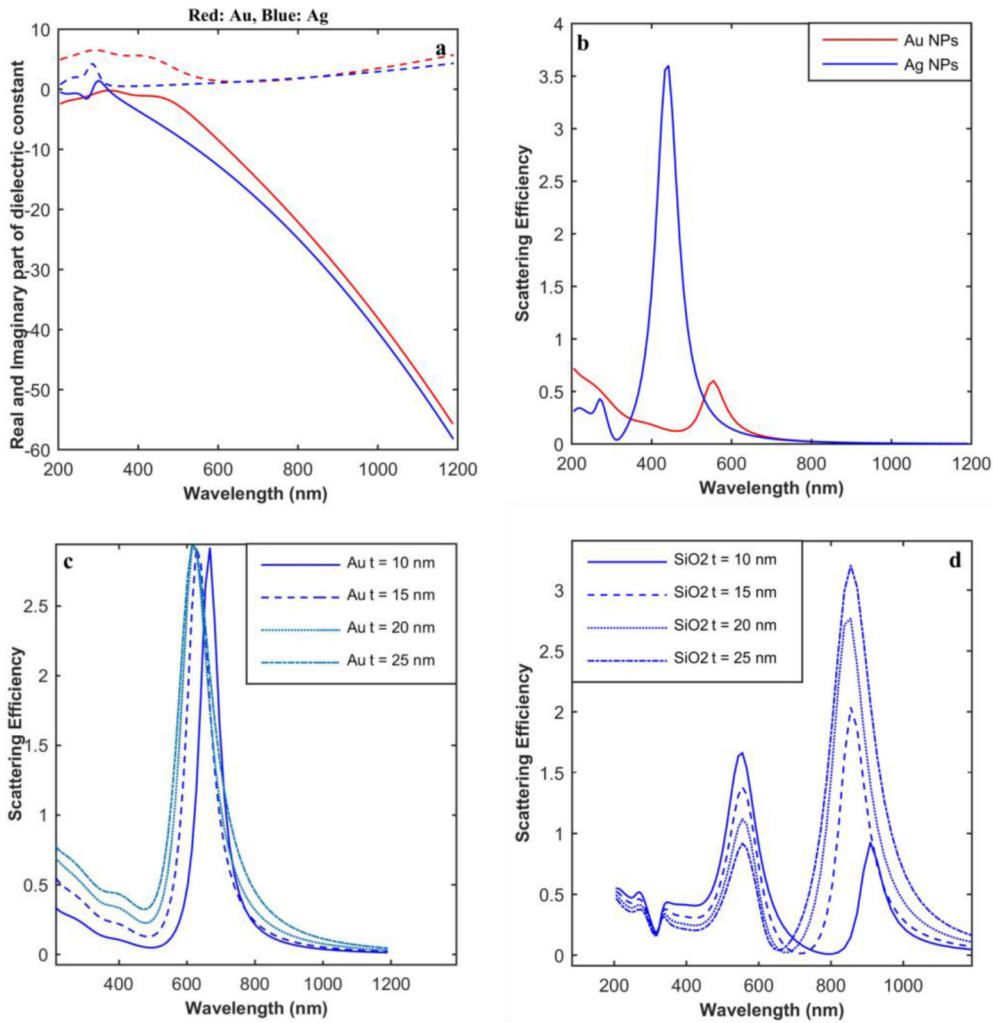


Fig. 3. Optical properties of different NPs: (a) Dielectric constants of NPs (Au, and Ag); (b) Au and Ag NPs with radius 30 nm scattering efficiency; (c) SiO₂/Au NPs scattering efficiency function of the Au thickness alteration; (d) Au/SiO₂/Ag NPs scattering efficiency function of the SiO₂ thickness alteration.

photon is either scattered or absorbed. It is notable when Δs is chosen in this manner, the photon is forced either to scatter or be absorbed after each propagation step [24]:

$$\Delta s = -\ln(rand)/(\mu_a + \mu_s) \quad (2)$$

Moreover, the probability that the photon is scattered is equal to the ratio of the scattering coefficients over the sum of the absorption and scattering coefficients. For this, ξ is a random number produced between 0 and 1, so the photon is scattered if:

$$\xi < \mu_s/(\mu_a + \mu_s) \quad (3)$$

Otherwise the photon is absorbed. If a photon is

scattered then a new photon direction is chosen based on the phase function. Otherwise, the photon is absorbed and the absorption position is considered for a new fluorescence photon which is emitted. In each photon trajectories, because of two different categories of the optical properties (I. tissue and II. tumor or NPs), we used the fNPs as the MC weight constant after each Δs determined as:

$$Ingredient\ type : \begin{cases} tumor/ NPs & f_{NPs} \times rand(1) > 0.5 \\ tissue & f_{NPs} \times rand(1) \leq 0.5 \end{cases} \quad (4)$$

All of these processes are described in the flowchart in figure 2. In the following, mechanics of the photon propagation in tissue are considered. With

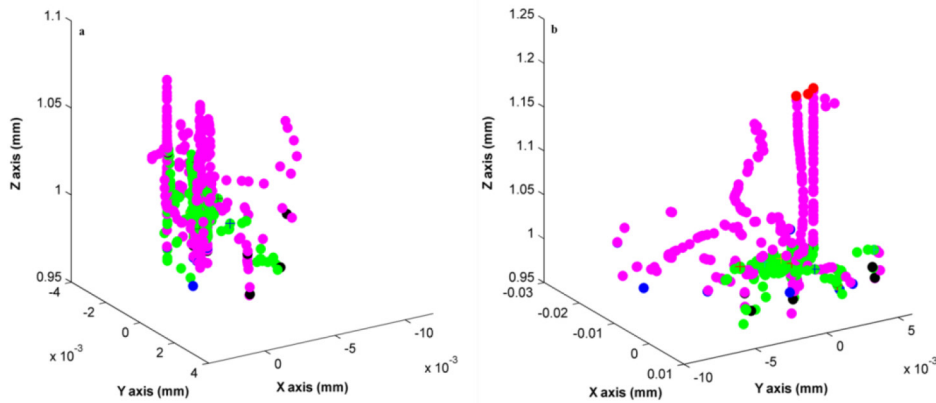


Fig. 4. X, Y, Z (cm) (a) FNPs=0.08; (b) FNPs=0.98: for better illustration the number of photons are considered 20; Yellow: Start Point; Green: Excitation Scattering; Magenta: Fluorescence Scattering; Blue: Diffuse Reflection; Black: Total Reflection; Red: Transmission; +: Excitation Photon Absorption which is converted to fluorescence emission at different wavelength.

regard to the work's algorithm, a photon is uniquely described by the five variables: three spatial coordinates for the position and two directional angles. In our study, the cylindrical coordinates were chosen for symmetry reasons. The direction cosines are simplified by taking the cosine of the angle that the photon direction makes with the each axis. These are specified by μ_x , μ_y , and μ_z relating to each of the x-, y-, and z- axes, respectively. So the new coordinates (x',y',z') are given by:

$$x' = x + \mu_x \Delta s, \quad y' = y + \mu_y \Delta s, \quad z' = z + \mu_z \Delta s \quad (5)$$

If a photon is scattered from direction (μ_x, μ_y, μ_z) by angle (θ, ϕ), so the new direction is specified by [24, 25]:

$$\begin{aligned} \mu_y' &= (\sin \theta / \sqrt{1 - \mu_z^2}) (\mu_y \mu_z \cos \phi + \mu_x \sin \phi) + \mu_y \cos \theta, \\ \mu_z' &= (-\cos \phi \sin \theta \sqrt{1 - \mu_z^2}) + \mu_z \cos \theta \end{aligned} \quad (6)$$

$$g = \int_{4\pi} p(s, s') \cdot (s, s') d\omega \quad (7)$$

Notably, any phase functions may be used with the MC method. The phase function describes the angular distribution for a single scattering event. For traceability, the phase function is usually assumed to be a function of the angle between s and s' (s and s' are the scattering direction). A normalized phase function describes the probability density function for the angle at which a photon is scattered. Moreover, anisotropic scattering is characterized by a non-uniform density function. In most cases, the form of the phase function is not known. However, the phase function is usually characterized by the average cosine of the phase function introduced by [24]:

$$g = \int_{4\pi} p(s, s') \cdot (s, s') d\omega \quad (7)$$

Generally, the phase function is different from particle to particle, so in the most cases, the average of the phase function has been used for simplicity. This parameter is usually called the anisotropy coefficient. It is a measure of the asymmetry of the single scattering pattern and in fact g can approach to 1, 0, and -1 describe purely forwarding, isotropic, and highly backward scattering, respectively. In the following, we discuss the possibility of internal reflection occurrence when the photon is propagated across an index of the refraction discontinuity. The reflection will only occur at the boundaries of the medium. The probability which a photon will be reflected is determined by the Fresnel reflection equation [24]:

$$\begin{aligned} R(\theta_i) &= 0.5 \cdot [(\sin^2(\theta_i - \theta_t) / \sin^2(\theta_i + \theta_t)) \\ &\quad + (\tan^2(\theta_i - \theta_t) / \tan^2(\theta_i + \theta_t))] \end{aligned} \quad (8)$$

where $\theta_i = \cos^{-1}(\mu_z)$ is the angle of incidence of the boundary and the angle of transmission θ_t is given by Snell's law:

$$n_i \cdot \sin \theta_i = n_t \cdot \sin \theta_t \quad (9)$$

where n_i and n_t are the indices of the refraction of the medium from which the photon is incident and transmitted, respectively. In the following, we need to examine the cosine of scattering angle as an important key in the case of light penetration. It is mentioned that the amount of this parameter alters between -1 and 1 whereby for light penetration enhancing the anisotropy factor should select

Table 1. Optical properties of real tissue (Liver: Murine) [25].

	μ_a	μ_s	(g)
At Excitation Wavelength(nm)	12.2	173.5	0.93
At Fluorescence Wavelength (nm)	6.5	143.7	0.95

Table 2. Optical properties of real tissue (R3327-AT) [25].

	μ_a (1/cm)	μ_s (1/cm)	(g)
Excitation Wavelength (nm)	0.49	270	0.975
Fluorescence Wavelength (nm)	0.49	270	0.975

Table 3. Optical properties of NPs Calculated by MIE theory.

	Wavelength (nm)	R _{core} (nm)	R _{shellI} (nm)	R _{shellII} (nm)	g _{NPs} (-)	abs_Eff (%)	sca_Eff (%)
NP _{sE} : Au/SiO ₂ /Ag	581	30	10	10	0.92	0.43	1.56
NP _{sF} : SiO ₂ /Au	621	30	10	-	0.998	0.58	2.45

close to 1. Interestingly, it should be noted that in the homogenous scattering the probability of the absorption dramatically increased [25, 26]. This parameter was presented in details in appendix 1.

SIMULATIONS AND RESULTS

We mentioned that, for manipulating the tissue’s optical properties, two types of core/shell NPs (NP_{sE}: Au/SiO₂/Ag and NP_{sF}: SiO₂/Au linked with dye molecule) are considered. The tissue, tumor, and NPs’ optical properties are found in table 1, 2, and 3 respectively. It is notable that the NP_{sE} are used in the excitation wavelength and are designed to have gNPs = 0.92. In this case, by controlling either the Au layer or SiO₂ shell thickness, the gNPs and SPR interactions between the inner and outer Au layers (SPR hybridization) could be engineered. The results of simulations show that the maximum gNPs occurred in the maximum state of SPR interactions, or equivalently in the small thickness of the SiO₂ spacer layer. In the following, the NP_{sF} are used to produce simultaneously a maximum SPR in the fluorescence wavelength and gNPs = 0.99. The original aim of this article is related to increase of the light penetration depth into a tissue, which is indirectly and transiently done by the alteration of the tissue’s optical properties. The indirect approach is used because we could not alter the optical properties of the real tissue directly. So it seems that by transiently inserting the NPs as dopants into tissue (see fig. 1b), its effective optical properties

are changed based on the NPs’ optical properties. It is noteworthy that the fraction of the inserting NPs must be controlled to avoid changing the tissue to another medium. In this work, approximately ~109 particles/mL NPs are used for calculation of the absorption and scattering coefficients. Moreover, the optical properties of the inserting NPs are easily manipulated, and their parameters such as μ_{aNP} , μ_{sNP} , and gNPs could be altered based on the NPs’ size and shape. Notably, when gNPs is selected to approach 1, the direction of the scattering is focused in the forward direction; therefore, by reducing the scattering events, the probability of the photon’s losses is severely decreased. In figure 2, the MC algorithm, used in this work, is illustrated. This algorithm consists of two distinct sections: one of them is related to the excitation section (left chart) and the other (right section) is attributed to the fluorescence. The different parameters such as the scattering, absorption, total reflection, diffuse reflection, and transmission are significant outputs of the simulations which are perused in this algorithm. Furthermore, a detector with a particular specification (Tables 4 and 5) is located in the defined position to collect the transmitted photons.

In figure 3, the optical properties of the NPs including SiO₂/Au and Au/SiO₂/Ag are illustrated. It is mentioned that by changing the NPs’ type, core and shell thickness, the optical parameters of the NPs could be manipulated. In figure 3a the dielectric constants (real and imaginary parts)

Table 4. Photon number detected by detector in tissue's depth= 2 mm calculated by Monte Carlo method.

Number of photon=15000; Tissue depth= 2mm; Tissue Width= 2 mm ; Detector position= (1 mm, 1 mm, 2 mm); Detector diameter= 0.5 mm; Detector Height= 4 mm; Initial position of photon= (0,0,1); Initial direction of photon= (9e-5,9e-5,0.99); n ₁ =1; n ₂ =1.37						
	Run 1	Run 2	Run 3	Run 4	Run 5	Avg
F_{NPs}=0.08 ; g _{NPs} =0.95; μ _{aNPs} =5; μ _{sNPs} =250; FOV=30;	60	46	47	65	64	56.4
F_{NPs}=0.58 ; g _{NPs} =0.95; μ _{aNPs} =5; μ _{sNPs} =250; FOV=30;	139	158	151	141	131	144
F_{NPs}=0.98 ; g _{NPs} =0.95; μ _{aNPs} =5; μ _{sNPs} =250; FOV=30;	215	383	225	346	358	305
F_{NPs}=0.98 ; g _{NPs} =0.95; μ_{aNPs}=50 ; μ _{sNPs} =250; FOV=30;	508	533	365	519	373	459.6
F_{NPs}=0.98 ; g _{NPs} =0.95; μ _{aNPs} =5; μ_{sNPs}=1000 ; FOV=30;	72	107	82	88	360	141.8
F_{NPs}=0.98 ; g_{NPs}=0.99 ; μ _{aNPs} =5; μ _{sNPs} =250; FOV=30;	575	368	627	567	589	545.2
F_{NPs}=0.98 ; g _{NPs} =0.95; μ _{aNPs} =5; μ _{sNPs} =250; FOV=60 ;	347	372	360	392	401	374.4

Table 5. Photon number detected by detector in tissue's depth= 4 and 5 mm calculated by Monte Carlo method.

Number of photon=15000; Tissue depth= 4 and 5mm; Tissue Width= 4 mm ; Detector position= (1 mm, 1 mm, 2 mm); Detector diameter= 0.5 mm; Detector Height= 4 mm; Initial position of photon= (0,0,1); Initial direction of photon= (9e-5,9e-5,0.99); n ₁ =1; n ₂ =1.37; FOV=30						
	Run 1	Run 2	Run 3	Run 4	Run 5	Avg
F _{NPs} =0.98; g_{NPs}=0.99 ; μ _{aNPs} =5; μ _{sNPs} =250; g _{NPs*} =0.99; μ _{aNPs*} =2; μ _{sNPs*} =150	3	1	2	1	2	1.8
F _{NPs} =0.98; g _{NPs} =0.95; μ_{aNPs}=50 ; μ _{sNPs} =250; g _{NPs*} =0.99; μ _{aNPs*} =2; μ _{sNPs*} =150	4	6	1	3	4	3.6
F _{NPs} =0.98; g_{NPs}=0.99 ; μ_{aNPs}=50 ; μ _{sNPs} =250; g _{NPs*} =0.99; μ _{aNPs*} =2; μ _{sNPs*} =150	2	1	1	2	1	1.4
F _{NPs} =0.98; g _{NPs} =0.95; μ_{aNPs}=50 ; μ _{sNPs} =250; g _{NPs*} =0.99; μ _{aNPs*} =2; μ_{sNPs*}=50	81	113	115	124	102	107
F _{NPs} =0.98; g _{NPs} =0.95; μ_{aNPs}=100 ; μ _{sNPs} =250; g _{NPs*} =0.99; μ _{aNPs*} =2; μ_{sNPs*}=50	69	72	69	66	74	70
F _{NPs} =0.98; g_{NPs}=0.99 ; μ _{aNPs} =5; μ _{sNPs} =250; g _{NPs*} =0.99; μ _{aNPs*} =2; μ_{sNPs*}=50	93	74	124	67	88	89.2
F _{NPs} =0.98; g _{NPs} =0.95; μ_{aNPs}=50 ; μ _{sNPs} =250; g _{NPs*} =0.99; μ _{aNPs*} =2; μ_{sNPs*}=50 ;	5	2	8	1	3	3.8

Tissue depth= 5 mm

of Au and Ag bulk materials are depicted. For comparison, we generally modeled the Au and Ag NPs' scattering efficiency (fig. 3b). Figures 3c, and 3d show the optical properties of Au/SiO₂ and Au/SiO₂/Ag NPs, which are designed to have gNPs = 0.92 and gNPs = 0.99, respectively. Additionally, to reach the optimum amount of scattering, absorption, and anisotropy factor, the NPs' radius is considered around 50 nm. These figures show that by alteration of the Au thickness (for example in SiO₂/Au NPs), the scattering has a blue shift which attributes to the changing interaction of light with the NPs. Moreover, this case is very interesting in Au/SiO₂/Ag NPs. In this case, by changing the SiO₂ thickness, the plasmon-plasmon interaction is altered, which leads to the shift of the NPs' plasmon resonance. So, by engineering the NPs' morphology, their plasmon resonance is managed. We selected these NPs due to their absorption and scattering profile in the considered wavelengths, by which they are effectively coupled to the fluorescence

agents; firstly, to increase the dye's quantum yield, and finally, to improve their fluorescence emission. In the following, the simulation results of the MC algorithm are illustrated. At first, for simplicity and a better illustration, the scattering trajectory and other important parameters for only 20 photons are illustrated in figure 4. In this figure, two distinct states are considered. One of them is related to fNps = 0.08. In the case of fig. 4a, the amount of inserting NPs is very low, so the optical properties of the tissue are predominant. In other words, the incident photons interacted mostly with the tissue's ingredients rather than the NPs when penetrated into the tissue. This means that their scattering trajectories are constructed based on the majority ingredients, which are tissue ingredients in this case. However, another case is considered for fNps = 0.98. In this case (fig. 4b), the maximum number of NPs (~109 particles/mL NPs) is inserted into the tissue. So, the incident photons have interaction with either tissue ingredients or NPs. It is shown

that in this figure, the photon penetration depth is dramatically increased. This contributes to the tissue's optical properties changing, which is indirectly done by the inserting of designed NPs into the tissue. Furthermore, in figure 4, the excitation scattering, fluorescence scattering, diffuse reflection, total reflection, transmission, and excitation photon absorption have been illustrated. Finally, in the similar way, but for 15,000 photons, some simulation results are presented in table 4 (tissue depth and width are considered to be 2 mm in this case) and table 5 (tissue depth and width is considered to be 4 and 5 mm). In table 4, the manipulations of the medium optical properties are done only by engineering the NPsE: Au/SiO₂/Ag without the second category of NPs. In this case the tissue depth and width are considered to be 2 mm. The data in this table shows that by altering the NPs' parameters including scattering efficiency, absorption efficiency, and the cosine of scattering angle and detector's field of view (FOV), the number of photons reaching the detectors could be changed. Subsequently, it is shown that using only the NPsE is not sufficient to increase the light penetration depth. In Table 5, in the three first rows, for 4 mm of the tissue depth, the alteration of just NPsE: Au/SiO₂/Ag is considered, and the influence of NPsF is ignored. It is clearly observable that the amounts of detected photons are severely decreased. However, in the other four rows, especially for 5 mm (the last row), besides NPsE, the other category of NPs is engineered based on article aims and its result is very interesting. It is noteworthy that these results for 5 mm thickness of a real tissue could satisfy the article's claim of an increase in light penetration depth. It should be noted that all of the data, which we used, were taken from an experimental article [25] and in fact, we simulated the light penetration into the tissue with the real and practical data.

CONCLUSIONS

In this article, the increasing of the light penetration depth into tissue (Liver: Murine) was investigated by engineering the optical properties of the core/shell NPs such as surface plasmon coupling. The simulation results show that increasing the light penetration depth into a tissue can be achieved if we can control and manage the effective optical parameters of the tissue (this does not mean a change of real tissue to the

other mediums, so, the concentration of inserted NPs must be controlled). The work's important conclusions are: (1) by controlling the gNPs, most of the scattering events' directions are forwardly aligned based on original aims; (2) the alteration of Au thickness layer, either in SiO₂/Au or Au/SiO₂/Ag, can affect SPR hybridization and also the optical parameters of the modified tissue (tissue and NPs); and (3) NPs' plasmon resonance severely affects the dyes' quantum yield and fluorescence emission. So, as an important result, the detection result for fNPs = 0.08 is 60 photons, and this case is increased to 215 photons for fNPs = 0.98, at 2 mm of real tissue. Finally, for NPs in the excitation wavelength, we should try to select a gNPs approaching 1, with the absorption efficiency simultaneously increasing to a high amount; however in the case of NPsF (NPs in the fluorescence wavelength) as well as selecting a forward direction for gNPs*, the scattering and absorption efficiency must be low to control the total loss..

CONFLICTS OF INTEREST

The authors declare that there are no conflicts of interest regarding the publication of this manuscript.

SUPPLEMENTARY MATERIAL

The Supplementary Material for this article can be found online at: http://www.nanomedicine-rj.com/jufile?ar_sfile=312340

REFERENCES

1. Xing Y, Zhao J, Conti PS, Chen K. Radiolabeled nanoparticles for multimodality tumor imaging. *Theranostics*, 2014;4 (3):290.
2. Chen K, Chen X. Design and development of molecular imaging probes. *Current topics in medicinal chemistry*, 2010;10 (12):1227-1236.
3. Zhao Q, Jiang H, Cao Z, Yang L, Mao H, Lipowska M. A handheld fluorescence molecular tomography system for intraoperative optical imaging of tumor margins. *Medical physics*, 2011;38 (11):5873-5878.
4. Tiwari DK, Tanaka S-I, Inouye Y, Yoshizawa K, Watanabe TM, Jin T. Synthesis and characterization of anti-HER2 antibody conjugated CdSe/CdZnS quantum dots for fluorescence imaging of breast cancer cells. *Sensors*, 2009;9 (11):9332-9354.
5. F Jiao P, Y Zhou H, X Chen L, Yan B. Cancer-targeting multifunctionalized gold nanoparticles in imaging and therapy. *Current medicinal chemistry*, 2011;18 (14):2086-2102.
6. SalmanOgli A. Nanobio applications of quantum dots in cancer: imaging, sensing, and targeting. *Cancer nanotechnology*, 2011;2 (1):1.
7. Gatenby RA, Gillies RJ. Why do cancers have high aerobic

- glycolysis? Nature reviews Cancer, 2004;4 (11):891.
8. Bardhan R. Nanostructures for plasmon enhanced fluorescence sensing: From photophysics to biomedicine: Rice University; 2010.
 9. SalmanOgli A, Rostami A. Simulation of tumor targeting enhancement by amplifying of targeted nano-biosensors radiation intensity. IEEE Transactions on Biomedical Engineering, 2013;60 (5):1328-1335.
 10. SalmanOgli A, Rostami A. Design and simulation of perturbed onion-like quantum-dot-quantum-well (CdSe/ZnS/CdSe/ZnS) and its influence on fluorescence resonance energy transfer mechanism. IET nanobiotechnology, 2013;7 (4):140-150.
 11. Killian JJ. Electrical properties of normal and transformed mammalian cells. Biophysical journal, 1984;45 (3):523-528.
 12. Graeber TG, Osmanian C, Jacks T, Housman DE. Hypoxia-mediated selection of cells with diminished apoptotic potential in solid tumours. nature, 1996;379 (6560):88.
 13. Ambrose E, James A, Lowick J. Differences between the electrical charge carried by normal and homologous tumour cells. nature, 1956;177 (4508):576-577.
 14. Fricke H, Morse S. The electric capacity of tumors of the breast. The Journal of Cancer Research, 1926;10 (3):340-376.
 15. Webb S, Sherratt J, Fish R. Mathematical modelling of tumor acidity: regulation of intracellular pH. Journal of theoretical biology, 1999;196 (2):237-250.
 16. Becker RO, Murray DG. The electrical control system regulating fracture healing in amphibians. Clinical orthopaedics and related research, 1970;73:169-198.
 17. Chiang M, Cragoe Jr E, Vanable Jr JW. Electrical fields in the vicinity of small wounds in *Notophthalmus viridescens* skin. The Biological Bulletin, 1989;176 (2S):179-183.
 18. Brewer AK, Passwater R. Physics of the cell membrane. Mechanisms involved in cancer. Am Lab, 1976;10:37-45.
 19. Dolgaleva K. Local-field effects and nanostructuring for controlling optical properties and enabling novel optical phenomena: University of Rochester; 2009.
 20. Quinten M. Beyond Mie's Theory II-The Generalized Mie Theory. Optical Properties of Nanoparticle Systems: Mie and beyond, 2011:317-339.
 21. SalmanOgli A, Rostami A. Plasmon modes hybridization influence on nano-bio-sensors specification. IEEE Transactions on Nanotechnology, 2013;12 (5):858-866.
 22. Deng Z-S, Liu J. Monte Carlo method to solve multidimensional bioheat transfer problem. Numerical Heat Transfer: Part B: Fundamentals, 2002;42 (6):543-567.
 23. Wilson B, Adam G. A Monte Carlo model for the absorption and flux distributions of light in tissue. Medical physics, 1983;10 (6):824-830.
 24. Prahl SA. Light transport in tissue. 1990.
 25. Cheong W-F, Prahl SA, Welch AJ. A review of the optical properties of biological tissues. IEEE journal of quantum electronics, 1990;26 (12):2166-2185.
 26. Joseph JH, Wiscombe W, Weinman J. The delta-Eddington approximation for radiative flux transfer. Journal of the Atmospheric Sciences, 1976;33 (12):2452-2459.